ChemPubSoc Europe
DOI: 10.1002/ejic.201600020
EurJIC European Journal of Inorganic Chemistry
Full Paper

Tuning of Perovskites

Wide-Range Tuning of the Mo Oxidation State in $La_{1-x}Sr_xFe_{2/3}Mo_{1/3}O_3$ Perovskites

Sergey Ya. Istomin,*[a] Varvara V. Chernova,[a] Evgeny V. Antipov,[a] Maxim V. Lobanov,[b] Ivan A. Bobrikov,[c] Viktor Yu. Yushankhai,[c] Anatoly M. Balagurov,[c] K. Y. Hsu,[d] J. -Y. Lin,[d] J. M. Chen,[e] J. F. Lee,[e] Olga S. Volkova,[a,f,g] and Alexander N. Vasiliev[a,f,g]

Abstract: $La_{1-x}Sr_xFe_{2/3}Mo_{1/3}O_3$ ($0 \le x \le 1$) perovskites allow exceptionally wide tuning of the Mo oxidation state from +3 (x = 0) to +6 (x = 1) with the Fe^{III} oxidation state virtually unchanged. The end members of this series show antiferromagnetic ordering in $LaFe_{2/3}Mo_{1/3}O_3$ at T_N = 520 K and ferrimagnetic ordering in $SrFe_{2/3}Mo_{1/3}O_3$ at T_C = 420 K. The crucial role of electron correlations in the Mo 4d shell suggests that $LaFe_{2/3}Mo_{1/3}O_3$ with a half-filled band is a Mott insulator, whereas $SrFe_{2/3}Mo_{1/3}O_3$ is a band insulator. In both cases, the magnetic structure is dictated by antiferromagnetic superexchange between localized magnetic moments. At intermediate compositions, an interplay of antiferromagnetic-superexchange and double-exchange interactions results in nonmonotonous variations of both the magnetic-ordering temperature and saturation magnetization.

Introduction

The double perovskite Sr_2FeMoO_6[1] exhibits ferromagnetic half-metallic properties with a Curie temperature T_C as high as 420 K and can be used for room-temperature tunnelling-type magnetoresistance (TMR) devices.[2] The magnitude of the tunnelling magnetoresistance is directly related to the spin polarization of the tunnelling electrons. Half-metals are unusual ferromagnets in which only half of the electrons (either spin up or spin down) participate in conductivity.[3] Although high values of spin polarization and tunnelling magnetoresistance have been measured at low temperatures, very small effects are usually found at room temperature.[4] The key factors responsible for the operation of spintronic devices are the ferromagnetic-ordering temperature and the saturation magnetization.[5] Therefore, many efforts have been made to increase these parameters by tuning the chemical composition of suitable compounds through either hole/electron doping or isovalent substitutions.[6]

The double perovskite Sr_2FeMoO_6 has a cubic (undistorted double perovskite, space group $Fm3m$) or tetragonal structure (space group $I4/m$, $a \approx \sqrt{2}a_{per}$, $c \approx 2a_{per}$) at room temperature, depending on the degree of antisite (Fe/Mo) disorder,[7] and the Fe and Mo cations have a chess-type ordering with a slight octahedral rotation along the c axis, as shown in Figure 1. This corresponds to the one-tilt $a^0a^0c^-$ system in the Glazer notation. In Sr_2FeMoO_6, the Fe cations are in a mixed oxidation state between +2 and +3, as observed from both ^{57}Fe Mössbauer spectroscopy[8] and Fe 2p3d resonant photoemission spectroscopy.[9]

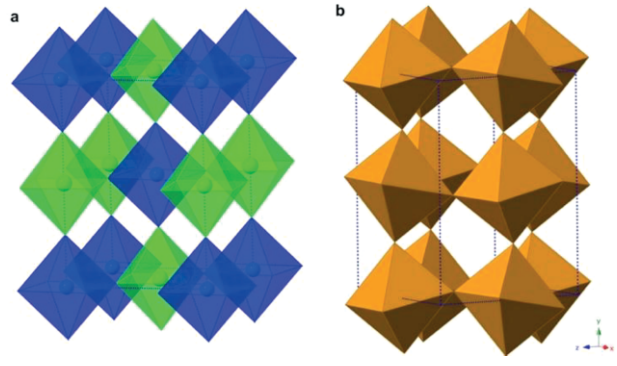

Figure 1. (a) The crystal structure of Sr_2FeMoO_6 with the Fe and Mo cations located in the blue and green octahedra, respectively. (b) The crystal structure of the orthorhombic perovskite $LaFe_{2/3}Mo_{1/3}O_3$ ($Pnma$, right). The A cations are not shown for clarity.

The electron doping of Sr_2FeMoO_6 through the partial substitution of the Sr^{2+} ions by La^{3+} ions in $Sr_{2-x}La_xFeMoO_6$ solid solutions is limited to x values close to 1.0 and results in the

[a] Moscow State University, Moscow 119991, Russia
E-mail: isserge71@gmail.com
www.chem.msu.ru
[b] All-Russian Scientific Research Institute of Aviation Materials, Moscow, 105005, Russia
[c] Joint Institute for Nuclear Research, Dubna 141980, Russia
[d] National Chiao Tung University, Hsinchu 30010, Taiwan
[e] National Synchrotron Radiation Research Center, Hsinchu 30076, Taiwan
[f] Ural Federal University, Yekaterinburg 620002, Russia
[g] National University of Science and Technology "MISiS", Moscow 119049, Russia
ORCID(s) from the author(s) for this article is/are available on the WWW under http://dx.doi.org/10.1002/ejic.201600020.

increase of T_C to 490 K (x = 1).[10] It has to be mentioned that the increase in the La content leads to a substantial decrease of the ordering of the B cations, and no ordering has been observed for compositions with $x > 0.8$.[11,12] A decrease of B-cation ordering is also observed in $Sr_{2-x}Nd_xFeMoO_6$.[13] This is not surprising because the close ionic radii of Fe^{3+} and Mo^{5+} [rFe^{3+} high spin (HS) = 0.645 Å, rMo^{5+} = 0.61 Å][14] results in the ordering of the Mo and Fe ions in Sr_2FeMoO_6 owing to the large charge-difference effect. Therefore, one can expect that the ordering of the Mo and Fe cations would decrease with decreasing Mo oxidation state (or with x in $Sr_{2-x}RE_xFeMoO_6$, RE = rare-earth cation). DFT calculations for the hypothetical compound La_2FeMoO_6 (x = 1) with formal oxidation states of Mo^{III} and Fe^{III} predict the stabilization of an antiferromagnetic ground state with T_N as high as 537 K.[15,16]

The variation of the Fe/Mo ratio in Sr_2FeMoO_6 according to formula $Sr_2Fe_{2-y}Mo_yO_6$ results in the preparation of perovskite-related oxides with no or partial ordering of the Fe and Mo cations depending on the x value and the preparation conditions. Fe-rich compositions exhibit large oxygen nonstoichiometry and crystallize with a brownmillerite-type structure with layered ordering of the oxygen vacancies.[17] The formation of ordered double perovskites with different octahedral tilting schemes has been observed for $0.5 \le y \le 1.2$,[18] whereas the study of compositions $0.75 \le y \le 2.0$ revealed the saturation of T_C at y = 0.95 and decreasing Curie temperature with increasing Mo content.[19] Popuri et al.[20] observed the absence of B-cation ordering for the y = 1.2 composition; $T_C \approx 250$ K was revealed by the magnetic susceptibility measurements, and G-type antiferromagnetic ordering was observed through room-temperature neutron powder diffraction (NPD) data. In recent theoretical studies supported by effective Hamiltonian calculations,[21–23] it was concluded that a possible way to increase the ferrimagnetic T_c without sacrificing the conduction electron polarization in Sr_2FeMoO_6 is the addition of excess Fe and the substitution of La on the Sr site to compensate for the loss of mobile carriers.

In the present paper, we report the syntheses, structures and a magnetic study of a new $La_{1-x}Sr_xFe_{2/3}Mo_{1/3}O_3$ ($0 \le x \le 1$) perovskite series. The limiting compositions with x = 0 ($LaFe_{2/3}Mo_{1/3}O_3$) and x = 1 ($SrFe_{2/3}Mo_{1/3}O_3$) have long been known. $LaFe_{2/3}Mo_{1/3}O_3$ has an orthorhombic perovskite structure [space group *Pnma*, $a \approx \sqrt{2}a_{per}$ = 5.6493(3) Å, $b \approx 2a_{per}$ = 7.9205(4) Å, $c \approx \sqrt{2}a_{per}$ = 5.5845(3) Å] with complete disorder of the B cations and exhibits high-temperature antiferromagnetism with $T_N \approx 520$ K.[24] In contrast, in the crystal structure of $SrFe_{2/3}Mo_{1/3}O_3$, there is a chess-type ordering of the B cations, and its chemical formula may be rewritten as $Sr_2(Fe)(Fe_{1/3}Mo_{2/3})O_6$ (space group *I4/m*, $a \approx \sqrt{2}a_{per}$, $c \approx 2a_{per}$ like Sr_2FeMoO_6 or space group *Fm3m*, $a \approx 2a_{per}$).[25] It is ferrimagnetic, and T_C varies between 280 and 500 K depending on the oxygen content.[26] Our X-ray absorption near-edge structure (XANES) study of $La_{1-x}Sr_xFe_{2/3}Mo_{1/3}O_3$ perovskites revealed that the Fe oxidation state remains close to +3 irrespective of x. Thus, in comparison with $Sr_{2-x}La_xFeMoO_6$ limited to $x \approx 1$ composition,[10] it is possible to vary the average oxidation state of Mo in a wide range from +3 for x = 0 to +6 for x = 1. This allows the magnetic properties of double perovskites to be tracked with the number of Mo 4d electrons.

Results

Single-phase samples of $La_{1-x}Sr_xFe_{2/3}Mo_{1/3}O_3$ were prepared for compositions $0.0 \le x \le 0.8$ and $SrFe_{2/3}Mo_{1/3}O_3$. It should be noted that samples with high amounts of lanthanum were prepared at 1150 °C, whereas lower temperatures were used to synthesize strontium-rich compositions. For example, single-phase samples of $SrFe_{2/3}Mo_{1/3}O_3$ were obtained at 1000 °C for 24 h. Attempts to synthesize single-phase samples with x = 0.9 were unsuccessful at various temperatures.

Owing to the low oxidation states of the B cations, samples of $La_{1-x}Sr_xFe_{2/3}Mo_{1/3}O_3$ demonstrate low stability in air at moderate temperatures. Thus, thermogravimetric (TG) studies of $LaFe_{2/3}Mo_{1/3}O_3$ and $La_{0.5}Sr_{0.5}Fe_{2/3}Mo_{1/3}O_3$ samples in air revealed weight gains at 325 and 350 °C, respectively. The analysis of the X-ray powder diffraction (XRPD) patterns of the samples after the TG study showed the formation of $La_2Mo_2O_9$ and $LaFeO_3$ for $LaFe_{2/3}Mo_{1/3}O_3$ and $SrMoO_4$ and $LaFeO_3$ for $La_{0.5}Sr_{0.5}Fe_{2/3}Mo_{1/3}O_3$. We observed only very small differences between the experimentally observed and calculated (given in brackets) weight gains of 2.93 (3.12) and 1.67 % (1.74) for the $LaFe_{2/3}Mo_{1/3}O_3$ and $La_{0.5}Sr_{0.5}Fe_{2/3}Mo_{1/3}O_3$ samples, respectively. This result indicates that only a small (if any) number of oxygen vacancies are formed in the crystal structures of the studied perovskites.

X-ray Powder Diffraction and Neutron Powder Diffraction

The XRPD patterns of the samples with $0 \le x < 0.8$ (Figure 2, A) were indexed for orthorhombic unit cells corresponding to the formation of $GdFeO_3$-type perovskite with space group *Pnma* ($a \approx \sqrt{2}a_{per}$, $b \approx 2a_{per}$, $c \approx \sqrt{2}a_{per}$), whereas the samples with x = 1 was indexed with a tetragonal unit cell with a = 5.577(2) Å and c = 7.841(3) Å. Owing to the presence of two competing trends, that is, the decrease of the B-cation size owing to the increase of its average oxidation state and the simultaneous increase of the A-cation average size owing to the larger ionic radius of Sr^{2+} (r = 1.44 Å) compared with that of La^{3+} (r = 1.36 Å),[14] only a slight variation of the unit-cell volume occurs with x. The small magnitude of the splitting of the perovskite substructure reflections together with the low intensity of the superstructure reflections [corresponding to orthorhombic supercell (O) $a \approx \sqrt{2}a_{per}$, $b \approx 2a_{per}$, $c \approx \sqrt{2}a_{per}$], especially observed for compositions with a large Sr content, significantly complicate the correct indexing of the XRPD patterns. The part of the XRPD patterns with a low-diffraction angle (2Θ = 15–30°), in which the majority of the strongest superstructure reflections are located, is shown in Figure 2 (B). The strongest superstructure reflection in the XRPD pattern of $LaFe_{2/3}Mo_{1/3}O_3$ is the $(111)_O$ reflection located at $2\Theta \approx 25°$. Its intensity decreases with increasing Sr content and it seems to disappear in the XRPD patterns of the samples with x = 0.8 and 1.0, as shown in Figure 2 (B). This indicates the formation of B-site-ordered perovskite phases for these compositions, as this reflection is

forbidden in both space groups *I4/m* ($a \approx \sqrt{2}a_{per}$, $c \approx 2a_{per}$) and *Fm3m* ($a \approx 2a_{per}$) reported for $SrFe_{2/3}Mo_{1/3}O_3$. At the same time, the $(011)_O$ reflection at $2\Theta \approx 19°$, which is absent in the XRPD patterns of the La-rich samples, becomes intense for compositions with $x \geq 0.5$.

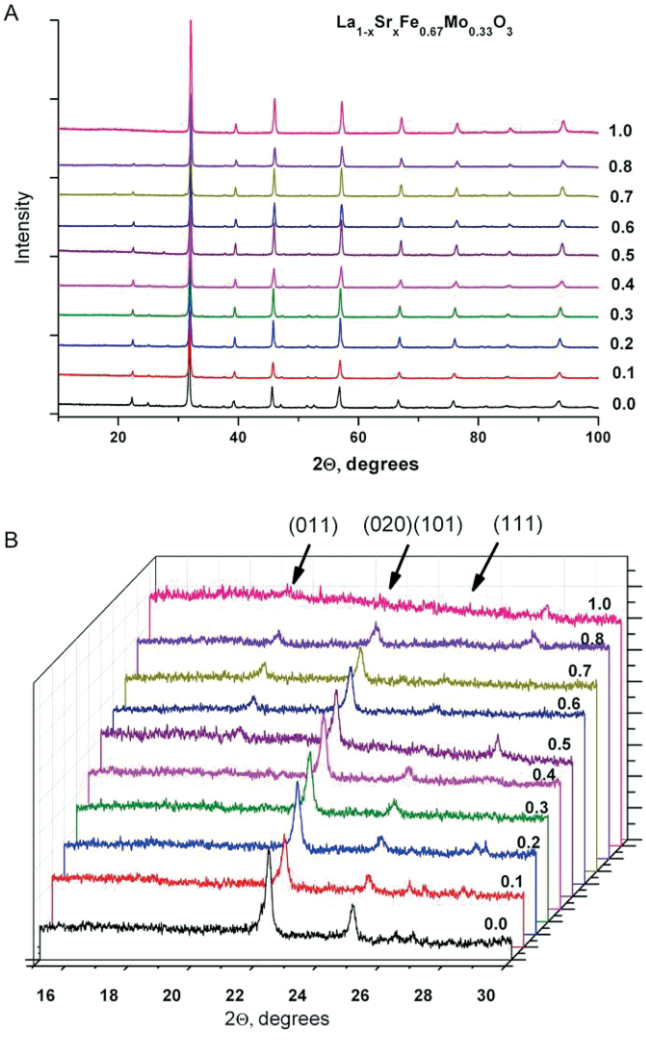

Figure 2. (A) XRPD patterns of $La_{1-x}Sr_xFe_{2/3}Mo_{1/3}O_3$ ($0.0 \leq x \leq 0.8$, $x = 1.0$). (B) Magnification of the part of the XRPD patterns in which the superstructure reflections are shown (see text). The indexes correspond to a unit cell with $a \approx \sqrt{2}a_{per}$, $b \approx 2a_{per}$, $c \approx \sqrt{2}a_{per}$.

The NPD data were obtained at 5 K (for $x = 0.5$ sample) and 293 K (for $x = 0.3$ and 0.5 samples). All of the diffraction peaks were indexed with the space group *Pnma*. No extra peaks were detected in the NPD patterns. A comparison of the diffraction intensities measured at different temperatures indicates the presence of only a G-type antiferromagnetic (AFM) contribution for the $x = 0.3$ sample and both ferromagnetic (FM) and G-type AFM contributions for the $x = 0.5$ sample. Simple calculations of the magnetic structural factors shows that the FM component of the magnetic structure for the *Pnma* space group contributes to the diffraction peaks with the even *k* Miller index, whereas AFM G-type ordering contributes to the odd *k* index. Thus both components can be refined independently. Similar conclusions were drawn after the analysis of the magnetic structure of Sr_2FeMoO_6 with ordered and disordered B cations.[7]

The presence of both FM and AFM components in the magnetic structure could be interpreted in several ways. The first possibility is a (weak) FM contribution in the canted AFM phase, which is allowed by symmetry for certain orientations of magnetic moment. Specifically, the allowed spin configurations containing both G and C components are $C_xG_yF_z$ (corresponding to Γ_2+ irreducible representation in Miller–Love notation) and $A_xF_yG_z$ (corresponding to Γ_4+). However, such canting is normally caused by a weak relativistic (Dzyaloshinskii–Moriya) term and cannot lead to the observed high magnitude of the FM moment. Consequently, this scenario could be excluded.

The second possibility is an incoherent mixture of FM and AFM phases, that is, mesoscopic separation onto the FM and AFM domains, which is plausible provided that the distribution of Fe and Mo over the B-cation sites is highly inhomogeneous. Alternatively, this could be explained by the formation of a long-range ferrimagnetic (FIM) structure. Clearly, the presence of a FIM structure suggests some degree of ordering of the Fe and Mo cations. Unfortunately, it is difficult to select between the last two models with the present NPD data restricted to the particular ($x = 0.5$) sample, as the refinements converged to very similar results. Nevertheless, strong evidence in favour of the AFM structure for low Sr concentration ($x < 0.4$) and the FIM structure for $0.4 < x \leq 1$ was obtained from the analysis of the macroscopic magnetic data. Such an analysis will be developed in detail in the Discussion section.

The final refinement of the atomic and magnetic structures in accordance with the neutron diffraction data was performed with two independent phases (atomic and magnetic: FIM). The results are shown in Figure 3 and reported in Table 1. The relative contributions of the crystal and magnetic structures in the diffraction patterns are shown in Figure 4. Owing to very small magnitude of the splitting of the perovskite subcell reflections for $La_{0.5}Sr_{0.5}Fe_{2/3}Mo_{1/3}O_3$ (the relative difference between the values of the lattice parameters is <0.3 %), it is impossible to

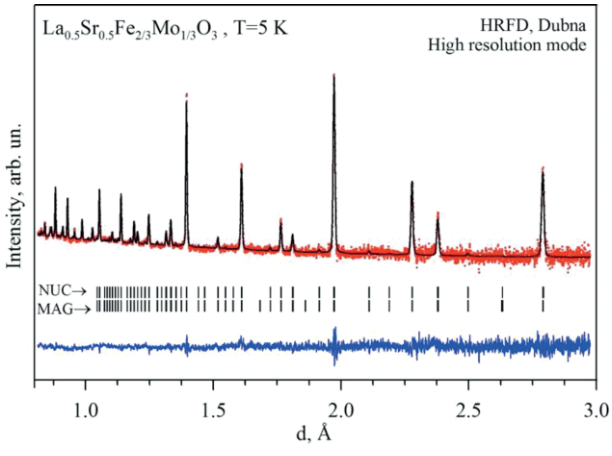

Figure 3. Observed and calculated NPD profiles of $La_{0.5}Sr_{0.5}Fe_{2/3}Mo_{1/3}O_3$ at 5 K and the difference between them. The refinement was performed with consideration of both magnetic and crystal structure. The vertical ticks indicate the calculated nuclear (upper row) and magnetic (lower row) reflection positions.

determine the direction of the magnetic moments with respect to the crystallographic axes.

Table 1. Summary of the results of the Rietveld fits of the NPD patterns, final atomic coordinates, and AFM and FM magnetic moments for $La_{1-x}Sr_xFe_{2/3}Mo_{1/3}O_3$ (x = 0.3 and 0.5) at room and low temperature. The thermal parameters of the cations were equated to each other. (La,Sr) and O1 are at 4c (x, 1/4, z); (Fe,Mo) are at 4b (0, 0, 1/2); O2 is at 8d (x, y, z).

	x = 0.3	x = 0.5	
T [K]	293	5	293
χ^2	1.01	2.31	1.93
R_w [%]	8.6	8.6	10.4
a [Å]	5.5923(3)	5.5754(1)	5.5842(2)
b [Å]	7.8921(3)	7.8647(1)	7.8830(2)
c [Å]	5.5867(3)	5.5623(1)	5.5803(2)
x(La/Sr)	0.0245(5)	0.0246(3)	0.0221(5)
z(La/Sr)	−0.0098(10)	−0.0044(8)	−0.0103(5)
B(La/Sr) [Å^2]	0.47(2)	0.41(1)	0.34(2)
B(Fe/Mo) [Å^2]	0.47(2)	0.41(1)	0.34(2)
x(O1)	0.4950(13)	0.4967(7)	0.5010(11)
z(O1)	0.0435(8)	0.0662(5)	0.0404(7)
B(O1) [Å^2]	0.57(7)	0.67(4)	1.01(7)
x(O2)	0.2793(8)	0.2671(4)	0.2664(9)
y(O2)	0.0457(4)	0.0284(2)	0.0312(3)
z(O2)	0.7278(9)	0.7245(4)	0.7306(11)
B(O2) [Å^2]	0.95(5)	0.57(2)	1.05(4)
μ_{AFM} [μ_B]	2.9(1)	3.24(7)	2.6(1)
μ_{FM} [μ_B]	ca. 0	2.2(2)	1.3(3)

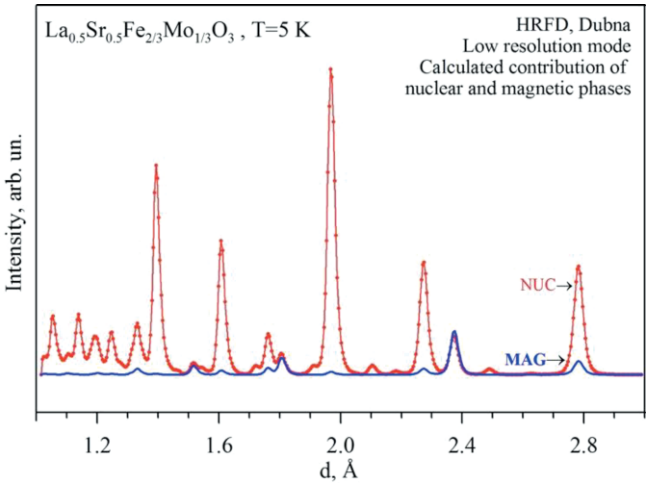

Figure 4. Calculated low-temperature neutron diffraction pattern of $La_{0.5}Sr_{0.5}Fe_{2/3}Mo_{1/3}O_3$ with contributions from crystal and magnetic structures. The contribution of the magnetic structure is significant in this d-spacing range.

As ferrimagnetic order (as proposed from the analysis of the macroscopic magnetization data for $x > 0.4$) is incompatible with *Pnma* symmetry, it is plausible that the actual symmetry is lower than *Pnma*, most probably $P2_1/n$ with checkerboard ordering of the B cations. However, the high-resolution NPD data did not reveal any evidence of symmetry lowering, and no anomalies were observed in the refined magnitudes of the atomic displacement parameters (ADPs, Table 1); therefore, the structural distortion (if any exists) is very small. Furthermore, refinement attempts in the $P2_1/n$ structural model did not improve the fit quality compared to that for the *Pnma* model. Consequently, we present the results of the refinements of the *Pnma* structural model.

Although the formation of B-site-ordered perovskite phases was confirmed for x = 0.8 and 1, the evaluation of the degree of Fe and Mo ordering in the compounds with lower La concentration ($0.0 \le x \le 0.7$) cannot be performed from the present XRPD studies of $La_{1-x}Sr_xFe_{2/3}Mo_{1/3}O_3$. Nevertheless, we argue below that some degree of B-cation ordering develops progressively for $x > 0.4$. This suggestion receives some indirect confirmation from the peculiar magnetic behaviour of $La_{1-x}Sr_xFe_{2/3}Mo_{1/3}O_3$, which is remarkably different for $x < 0.4$ and $x > 0.4$. This difference is argued to be intimately related to the Fe and Mo ordering over the B-cation lattice, which occurs for $x > 0.4$. The formation of B-site-ordered double perovskites $A_2BB'O_6$ is dictated by the disparity between the average charges of the B and B′ cations, their ionic radii, cation coordination geometry and A-cation/B-cation size difference.[27] For $La_{1-x}Sr_xFe_{2/3}Mo_{1/3}O_3$ perovskites, the increase in charge difference with x should be the predominant factor, as the ionic radius of Fe^{3+} (r = 0.645 Å) is rather close to those of both Mo^{3+} (r = 0.67 Å) and Mo^{6+} (r = 0.60 Å).[14]

X-ray Absorption Near-Edge Structure

To reveal the Fe oxidation state, the Fe-*K*-edge XANES spectra of $LaFe_{2/3}Mo_{1/3}O_3$ and $SrFe_{2/3}Mo_{1/3}O_3$ together with those of the standard samples FeO (Fe^{2+}), Fe_3O_4 ($Fe^{2.66+}$) and Fe_2O_3 (Fe^{3+}) were recorded, as shown in Figure 5 (A). Although the spectra show distinct edge energies for the standard samples owing to the various oxidation states, the Fe-*K*-edge energies of $LaFe_{2/3}Mo_{1/3}O_3$ and $SrFe_{2/3}Mo_{1/3}O_3$ are very close to each other, which suggests that they have a similar Fe oxidation state. This is the case for all $La_{1-x}Sr_xFe_{2/3}Mo_{1/3}O_3$ perovskites, as shown in Figure 5 (B). To be more quantitative, the edge energy can be defined according to the inflection of the edge in the spectrum. The Fe-*K*-edge energies of all samples are depicted in Figure 6. These results clearly demonstrate that the oxidation state of the Fe cations in $La_{1-x}Sr_xFe_{2/3}Mo_{1/3}O_3$ is very close to +3 for all studied compositions.

With a nearly constant oxidation state of Fe^{III}, one can expect the oxidation state of Mo cations to vary from +3 in $LaFe_{2/3}Mo_{1/3}O_3$ to +6 in $SrFe_{2/3}Mo_{1/3}O_3$ with increasing x. To verify this scenario, the Mo-*K*-edge spectra of $LaFe_{2/3}Mo_{1/3}O_3$ and $SrFe_{2/3}Mo_{1/3}O_3$ together with those of the standard samples Mo, MoO_2, MoO_3 and $La_{1-x}Sr_xFe_{2/3}Mo_{1/3}O_3$ are shown in Figure 7 (A). Moreover, the Mo-*K*-edge spectra of all $La_{1-x}Sr_xFe_{2/3}Mo_{1/3}O_3$ samples are shown in Figure 7 (B). For the Mo-*K*-edge, it was suggested that the second-peak energy, as indicated by the arrow in Figure 7 (B), serves as an appropriate reference to the Mo oxidation state.[28] According to this criterion, the consequent Mo oxidation state variation in $La_{1-x}Sr_xFe_{2/3}Mo_{1/3}O_3$ with x was explicitly observed, as shown in Figure 8. Indeed, the Mo oxidation state in $La_{1-x}Sr_xFe_{2/3}Mo_{1/3}O_3$ increases from +3 to +6 correspondingly with the value of x increasing from 0 to 1. It is noted from Figure 6 that the Fe oxidation state in all $La_{1-x}Sr_xFe_{2/3}Mo_{1/3}O$ all samples is generally slightly lower than +3. Similarly, the Mo

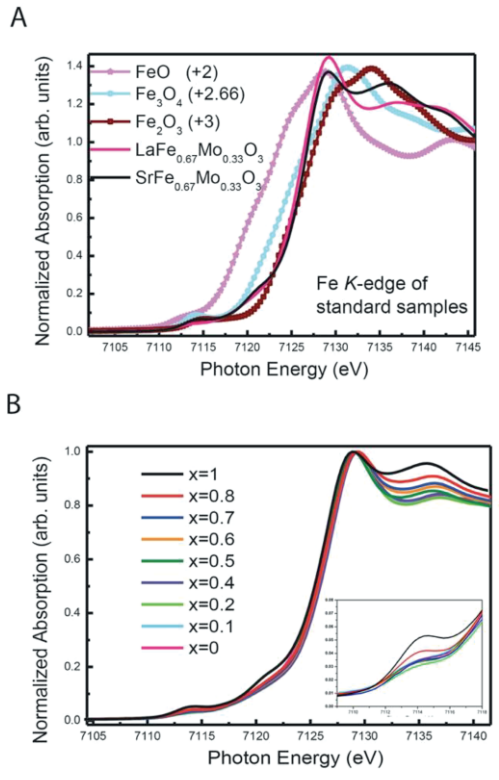

Figure 5. (A) Fe-*K*-edge XANES spectra of FeO (+2), Fe_3O_4 (+2.66), Fe_2O_3 (+3), $LaFe_{2/3}Mo_{1/3}O_3$ and $SrFe_{2/3}Mo_{1/3}O_3$ normalized between 7780 and 7830 eV; (B) Fe-*K*-edge XANES spectra of $La_{1-x}Sr_xFe_{2/3}Mo_{1/3}O_3$ ($0.0 \le x \le 1$) normalized at the peaks at ca. 7130 eV. The enlarged pre-edges are shown in the inset.

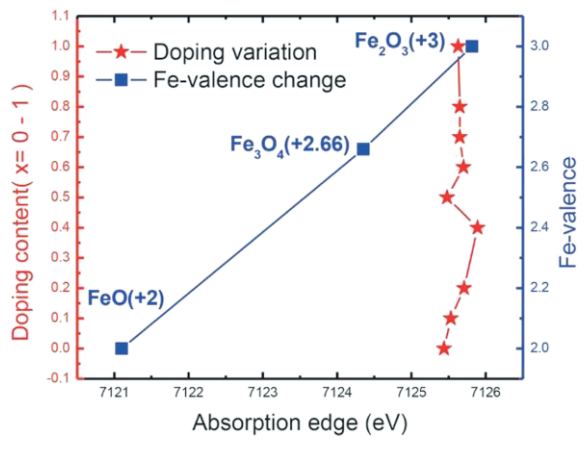

Figure 6. The Fe-*K*-edge energies of $La_{1-x}Sr_xFe_{2/3}Mo_{1/3}O_3$ and the standard samples. Left axis: the doping level *x* of Sr of $La_{1-x}Sr_xFe_{2/3}Mo_{1/3}O_3$. Right axis: Fe oxidation state of the standard samples.

oxidation state for all $La_{1-x}Sr_xFe_{2/3}Mo_{1/3}O_3$ samples is always slightly lower than the expected value from the Sr doping content *x*. It is plausible that these differences in the oxidation states can be attributed to a small oxygen deficiency in the samples, and the oxygen deficiency δ to achieve charge balance in $La_{1-x}Sr_xFe_{2/3}Mo_{1/3}O_{3-\delta}$ can be estimated. For the oxidation states of Fe and Mo shown in Figures 6 and 8, $\delta \le 0.08$ for all samples. This δ value is much smaller than $\delta = 0.3$ for $SrFe_{1.75/2}Mo_{0.25/2}O_{3-\delta}$, as reported in ref.[29]

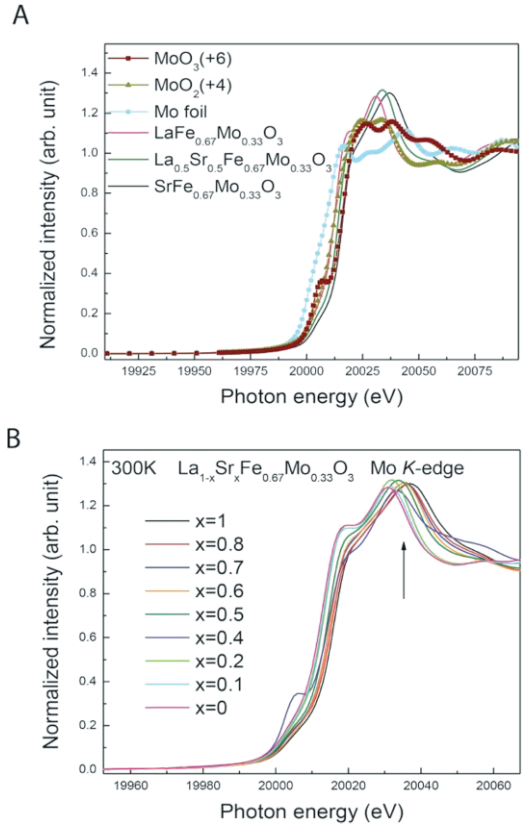

Figure 7. (A) The Mo-*K*-edge spectra of MoO_2 and MoO_3 compared with those of $La_{1-x}Sr_xFe_{2/3}Mo_{1/3}O_3$ (x = 0, 0.5, 1); (B) the Mo-*K*-edge spectra of $La_{1-x}Sr_xFe_{2/3}Mo_{1/3}O_3$ ($0.0 \le x \le 1$). All Mo-*K*-edge spectra are normalized between 20660 and 20710 eV.

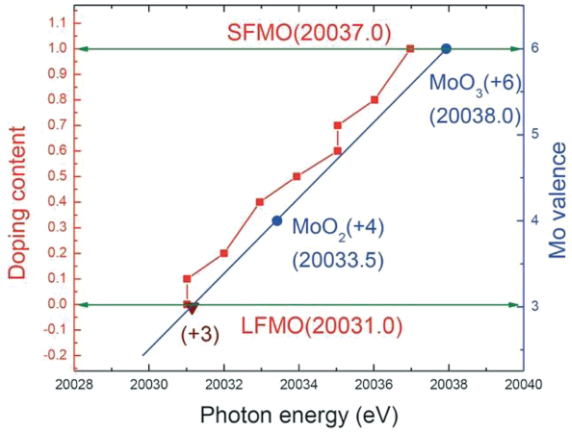

Figure 8. The second-peak energy of the Mo-*K*-edge spectra for $La_{1-x}Sr_xFe_{2/3}Mo_{1/3}O_3$ ($0.0 \le x \le 1$) and the standard samples. The *y* axis on the left shows the different doping content of Sr for $La_{1-x}Sr_xFe_{2/3}Mo_{1/3}O_3$, and the *y* axis on the right shows the oxidation state of the Mo standard samples. The Mo oxidation state increases with increasing Sr content.

The Fe K pre-edges in transition-metal oxides are caused by the hybridization of 3d and 4p states.[30] These are further enlarged in the inset of Figure 5 (B). All of the pre-edges show only one feature at ca. 7114 eV, which is ascribed to the Fe^{III} state, and further features at a lower energy for Fe^{II} are absent.[29] This concurs with the small δ value estimated

above and suggests that the Fe oxidation states of all $La_{1-x}Sr_xFe_{2/3}Mo_{1/3}O_3$ samples in Figure 6 are very close to +3. Furthermore, the pre-edges of the x = 1 and 0.8 samples are intriguingly more significant than those of the others (especially for x = 1). In general, an increase in the pre-edge intensity can be caused by a smaller coordination number for the Fe ion or enhanced distortion of the local octahedral structure.[29,30] In the present case, considering the absence of Fe^{II} features, the significantly enhanced Fe K pre-edge more likely manifests a unique octahedral distortion of the Fe environment for the end compounds. The changes of the spectra at ca. 7120 eV in Figure 5 are probably caused by the same factor discussed above. The Mo K pre-edges at ca. 20005 eV in Figure 7 (B) are similar for all $La_{1-x}Sr_xFe_{2/3}Mo_{1/3}O_3$ samples and are somewhat less significant than those of the Fe-*K*-edge (with the exception of x = 0.4, possibly because of a particular decrease in the coordination number of Mo for an unknown reason). These results imply that the local octahedron of the Mo ions experiences less distortion than that of the Fe ions even for the end compounds.

To conclude, the oxidation state of the Fe cations in $La_{1-x}Sr_xFe_{2/3}Mo_{1/3}O_3$ remains almost constant at close to +3, whereas the Mo oxidation state from +3 to +6 as x increases from 0 to 1. Therefore, the XANES results prove that the engineering of the Mo oxidation state is realized, and the magnetic properties of $La_{1-x}Sr_xFe_{2/3}Mo_{1/3}O_3$ can be further explored on a firm base.

Magnetization

The temperature dependence of the reduced magnetization M/B of $LaFe_{2/3}Mo_{1/3}O_3$ with Fe^{3+} and Mo^{3+} ions is shown in the upper panel of Figure 9. Two peaks at T_1 = 527 K and T_2 = 130 K are clearly seen. As the magnetization decreases below both these temperatures, these transitions can be considered as antiferromagnetic ones. Furthermore, the magnetization curve measured at 2 K demonstrates a spin-flop-like feature at B_C = 2.8 T (see upper panel of Figure 9), which indicates the effects of magnetic anisotropy.

As suggested and discussed below in more detail, the formation of AFM ordering in $LaFe_{2/3}Mo_{1/3}O_3$ is the result of the interplay of several specific factors. First, owing to their Fe^{3+} and Mo^{3+} ionic states, these ions are distributed statistically over the B-cation lattice, and the AFM superexchange interaction between numerous pairs of neighbouring Fe magnetic moments becomes dominant because of the excess of Fe over Mo. Moreover, we suggest that $LaFe_{2/3}Mo_{1/3}O_3$ is an insulating material in which localized moments in Mo^{+3}–Mo^{+3} and Mo^{+3}–Fe^{+3} pairs of neighbouring ions are also coupled by AFM superexchange, as follows from the Goodenough–Kanamori–Anderson (GKA) rules. In this respect, the nature of the AFM ordering in $LaFe_{2/3}Mo_{1/3}O_3$ is different from the hypothetical one predicted in refs.[15,31] for double perovskites $La_{1-x}Sr_xFe_{1/2}Mo_{1/2}O_3$ as x tends to zero.

The replacement of even a small amount of lanthanum in $LaFe_{2/3}Mo_{1/3}O_3$ by strontium changes the response to the external magnetic field considerably. In particular, as seen in the upper panel of Figure 9, the high-temperature anomaly for

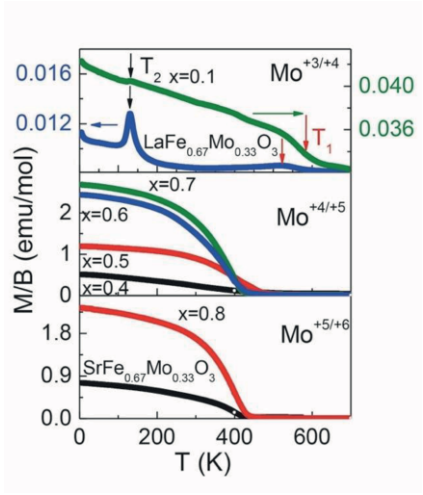

Figure 9. The temperature dependencies of the reduced magnetization M/B of $La_{1-x}Sr_xFe_{2/3}Mo_{1/3}O_3$ compounds measured at B = 0.1 T. The vertical arrows are a guide to highlight the magnetic phase transitions. The Mo oxidation state is indicated in the top right corner of each panel.

$La_{0.9}Sr_{0.1}Fe_{2/3}Mo_{1/3}O_3$ at T_1 transforms into a steplike increase of reduced magnetization, whereas the anomaly at T_2 is suppressed, and the reduced magnetization of $La_{0.9}Sr_{0.1}Fe_{2/3}Mo_{1/3}O_3$ increases almost four times in comparison with that of the parent material (x = 0). We suggest that the enhanced magnetization indicates the appearance of an additional contribution from a readily spin-polarizable itinerant component on top of that from localized strongly coupled magnetic moments. In the ionic picture, the introduction of Sr^{2+} ions leads to the oxidation of molybdenum, that is, the appearance of Mo^{4+} ($4d^2$, S = 1) ions in the structure. In the band picture, this means that the occupancy n of the conduction band is reduced from n = 3 (x = 0) to n = 2.7 (x = 0.1), and the itinerant component can be viewed, for instance, as holes with concentration δn = 0.3 in the conduction band of the Mo network.

These processes evolve with the doping level until x = 1/3, which suggests that the oxidation states of the cations are equal according to $La^{3+}_{0.67}Sr^{2+}_{0.33}Fe^{3+}_{2/3}Mo^{4+}_{1/3}O_3$. For higher strontium concentrations, the growing fraction of Mo^{5+} ($3d^1$, S = 1/2) manifests itself in drastic changes to the magnetic properties. As shown in the middle panel of Figure 9 for $La_{1-x}Sr_xFe_{2/3}Mo_{1/3}O_3$ ($0.4 \le x \le 0.7$), the temperature dependences of the reduced magnetization under the external magnetic field demonstrate ferro-/ferrimagnetic-type increases as the temperature decreases, and the onset of magnetic ordering occurs in the same temperature interval of 410–450 K. The measured magnetization values are approximately two orders of magnitude larger than those for compounds with $x < 0.3$. Furthermore, the magnetization curves measured at 2 K (shown in the middle panel of Figure 10) demonstrate behaviour typical for ferro/ferrimagnets and reach saturation for $B > 3$ T. The values of saturated magnetization increase with strontium doping for $0.4 \le x \le 0.7$. As discussed below, these features are compatible with a scenario of a ferrimagnetic state with two-component magnetization formed by the localized Fe spins and the con-

duction electrons of the Mo network. In this scenario, the observed behaviour of saturation magnetization can be explained by consideration of a variation of the induced spin polarization of the conduction electrons that is dependent on the Sr content.

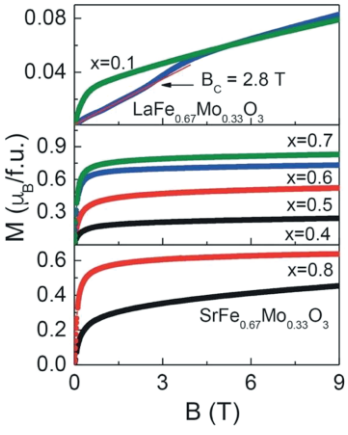

Figure 10. The field dependencies of the magnetization of $La_{1-x}Sr_xFe_{2/3}Mo_{1/3}O_3$ at T = 2 K. The solid line emphasizes the almost linear growth of the magnetization below the spin-flop-like transition at B_C marked by an arrow for $LaFe_{2/3}Mo_{1/3}O_3$.

For x = 2/3, the charge states of the ions are $La^{3+}{}_{0.33}Sr^{2+}{}_{0.67}Fe^{3+}{}_{2/3}Mo^{5+}{}_{1/3}O_3$. Therefore, a further increase of Sr content leads to the appearance of Mo^{6+} ($3d^0$, S = 0) ions and the structural ordering of Fe^{3+} and Mo^{6+} cations over the B-cation lattice for x = 0.8 and 1. The temperature dependences of the reduced magnetization M/B of $La_{1-x}Sr_xFe_{2/3}Mo_{1/3}O_3$ ($x > 0.7$) are shown in the lower panel of Figure 9. As in the previous case, $0.4 \le x \le 0.7$, the observed dependence of M/H versus T demonstrates ferro-/ferrimagnetic-type behaviour accompanied by a small decrease of T_C. The decrease of magnetization for both M/B versus T and M versus B corresponds well to the appearance of nonmagnetic Mo^{6+} ions, which also means a steady depletion of the conduction band down to n = 0 at x = 1, and this explains the decreased induced magnetization in these compounds. The evolution of the magnetization per unit cell with x is shown in Figure 10 (lower panel). In total, the

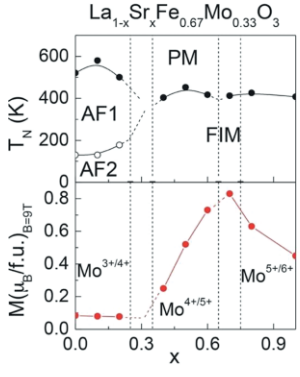

Figure 11. The upper panel represents the magnetic phase diagram of the $La_{1-x}Sr_xFe_{2/3}Mo_{1/3}O_3$ family of compounds. The solid lines separate paramagnetic and magneto-ordered regions. The lower panel represents the magnetic moments obtained under a 9 T magnetic field at 2 K. The vertical dashed lines indicate the critical values of x separating different Mo oxidation states.

data for the macroscopic magnetic characterization of $La_{1-x}Sr_xFe_{2/3}Mo_{1/3}O_3$ were used to reconstruct the "critical temperature–concentration" magnetic phase diagram, as shown in Figure 11 (upper panel).

Discussion

The microscopic mechanisms responsible for the peculiar magnetic behaviour of $La_{1-x}Sr_xFe_{2/3}Mo_{1/3}O_3$ can be understood by comparison with those of the well-studied double perovskites $La_{1-x}Sr_xFe_{1/2}Mo_{1/2}O_3$.[1,32,33] Below, we refer to both compounds as two members of the same family $La_{1-x}Sr_xFe_{1-y}Mo_yO_3$ with different Fe–Mo compositions, namely, y = 1/3 and y = 1/2, respectively. The common basis is a low-energy electronic model properly formulated in terms of the localized (core) spin S = 5/2 at the Fe sites and the conduction electrons on the network formed from the t_{2g} orbitals of the Mo ions. Here, the effective conduction bandwidth W_{eff} and the band filling n, controlled mainly by the composition (y) and Sr concentration (x), are important parameters of the problem. In general, several spin-coupling mechanisms present in the system in cooperation with effects of the band kinetic energy ($\approx nW_{eff}$) and electron correlations owing to on-site Coulomb repulsion (ca. U) together determine a specific low-temperature magnetic ordering, which depends on the Fe–Mo composition and the peculiarities of the Fe and Mo spatial distribution over the B-cation lattice sites.

In Sr-based (x = 1) double perovskites (y = 1/2) with Fe and Mo located in different sublattices of the B-cation lattice, the double-exchange-type interaction between nearest-neighbour (NN) Fe–Mo sites and the band kinetic-energy effects dominate; thus, a peculiar FIM state occurs, in which the large spins of the Fe ions are parallel, and the conduction-band spins of the Mo network are in the opposite direction.

The change of the composition between Fe and Mo from y = 1/2 to y = 1/3 introduces new aspects into the problem. Firstly, irrespective of the Sr/La concentration, the B-cation lattice can be considered as composed of two interpenetrating networks formed of Fe and Mo ions, respectively, and the number of NN Fe–Fe pairs in the Fe network is much higher than that of NN Mo–Mo pairs in the Mo network. The strength of superexchange J_{FF} between the neighbouring Fe core spins can be estimated from the Neel temperature T_N(LFO) = 750 K for similar perovskite $LaFeO_3$. On the basis of the mean-field expression $T_N(\text{LFO}) = zS(S + 1)J_{FF}/3k_B$, in which z = 6, S = 5/2, and k_B is the Boltzmann constant, one obtains $J_{FF} \approx 4$ meV. As will be argued below, the AFM coupling between the core spins in the massive Fe network becomes the dominant interaction that determines the main trends in the magnetic behaviour of $La_{1-x}Sr_xFe_{2/3}Mo_{1/3}O_3$ at any x. Simultaneously, the effective bandwidth W_{eff} of the conduction electrons and, hence, the band kinetic-energy effects in the loosened Mo network are reduced strongly in comparison with those of the double perovskites. For y = 1/3, the occupancy n of the t_{2g} subshell of Mo (i.e., the conduction-band filling) depends linearly on the Sr concentration, $n = 3(1 - x)$, and varies in a wider range from n = 3 ($t_{2g}{}^3$ configuration of Mo) at x = 0 to n = 0 ($t_{2g}{}^0$ configura-

tion) at $x = 1$, which corresponds to the limits of half-filled and empty bands, respectively.

Here, we emphasize the potentially crucial role of electron correlations[5,34] owing to considerable on-site Coulomb repulsion ($\approx U$) in the Mo 4d shell, which may be especially important in the limit of half-filling ($n = 3$) but are frequently disregarded in the theoretical analysis of double perovskites. In this limit, large U values may lead to the Mott insulating phase if the ratio U/W_{eff} exceeds the typical threshold $(U/W)_c \approx 1/2$, which is credible in $La_2Fe_{2/3}Mo_{1/3}O_3$, particularly in view of the reduced effective bandwidth W_{eff} mentioned earlier. In this case, the conduction electrons are probably localized with high spin $S = 3/2$ owing to the intra-atomic Hund interaction in the t_{2g}^3 configuration of Mo.

On the basis of the above arguments for the correlated conduction electrons in $La_{1-x}Sr_xFe_{2/3}Mo_{1/3}O_3$, one expects a crossover between two regimes of their behaviour in dependence on the Sr concentration x and, hence, on the band filling $n = 3(1 - x)$. The first regime, designated hereafter as the correlated one, is for $2 < n \leq 3$, that is, at and near to the half-filling. At $n = 3$, the pronounced electron correlations strive to create a localized Mo high-spin state that is coupled to the neighbouring moments of Fe and Mo with the coupling constants J_{Fe-Mo} and J_{Mo-Mo}, respectively. The AFM nature of the magnetic interaction in NN Fe–Mo and Mo–Mo pairs is similar to that of NN Fe–Fe pairs, as can be proved with the use of the standard concepts of the superexchange theory. In each pair of NN cations sharing a common oxygen atom, the superexchange path along the (nearly) 180° bond connects the half-filled t_{2g} orbitals of both cations. If the conduction-band occupancy deviates slightly from the half-filled limit, that is, $n = 3 - \delta n$ ($\delta n \approx 0.1$), the ground state of the system is no more an insulating one but can be still regarded as a state with "nearly localized" Mo magnetic moments with a small admixture ($\delta n \approx 0.1$) of itinerant degrees of freedom. This consideration is helpful in understanding the difference in the character of the magnetic susceptibility as a function of temperature at $x = 0$ and at low but finite Sr concentration ($x = 0.1$), as clearly seen in the upper panel of Figure 9. The second regime, regarded as the itinerant one, is for $0 < n < 2$, in which the correlation effects are typically weakened,[5,34] and the delocalized spin densities of the conduction electrons of the Mo network are antiferromagnetically coupled to the local Fe spins and prefer to follow (with opposite sign) the spatial spin distribution dictated by the massive network of Fe cations. Only this double-exchange-type Mo–Fe coupling and strong AFM NN Fe–Fe superexchange determine the overall magnetic development in the entire system $La_{1-x}Sr_xFe_{2/3}Mo_{1/3}O_3$ with delocalized band electrons for $x > 1/3$.

To be more precise, consider first the limit $x = 0$, for which the formal ionic charges of Fe^{3+} and Mo^{3+} are the same, and one expects full structural disorder in the distribution of both ions over the B-cation sites in the perovskite lattice. As the site-occupancy probabilities of 2/3 and 1/3 for Fe and Mo, respectively, are larger than the percolation threshold of 0.31, the percolation theory[35] allows us to consider each of two interpenetrating networks as containing a single infinite cluster and some amount of "isolated" ones. As in the dense $LaFeO_3$ system, the infinite Fe cluster tends to undergo the magnetic phase transition into the Neel-type ordered state but at the reduced temperature $T'_N \approx 0.6T_N(LSO) = 450$ K. Here, the factor 0.6 is for the reduced concentration (2/3) of interacting spins located on the sites of a simple cubic lattice.[35] As (1) the Mo network is expected to be in a strongly correlated regime with high spin $S = 3/2$ localized on Mo sites and (2) the overall compliance of all NN exchange interactions J_{FF}, J_{MM} and J_{FM} (i.e., all NN exchanges are of AFM character), we conclude that the $LaFe_{2/3}Mo_{1/3}O_3$ system should display properties of a two-sublattice AFM pattern with the complete compensation of the sublattice magnetizations because of the random distribution of Fe and Mo over both sublattices in the B-cation (nearly) cubic lattice. The ordering temperature is expected to be higher than the above estimate, that is $T_N > T'_N$, because of the mutually supportive NN AFM interactions in the entire system.

It is tempting to recognize the broadened peak at $T_1 = 527$ K, seen in the upper panel of Figure 9, as the onset of the Neel transition in $LaFe_{2/3}Mo_{1/3}O_3$. However, the broadening of this peak and the presence of a second sharp peak at $T_2 = 130$ K indicate the more complex two-step nature of the magnetic ordering, which is not captured in the simple intuitive picture developed above. The complexity has several sources including (1) the percolating character of the Fe and Mo networks, which is probably responsible for the broadening of the high-temperature peak at $T_1 = 527$ K, and (2) the potentially important role of the spin anisotropy in determining the peculiar low-temperature magnetic structure. The complexities introduced by the aforementioned effects deserve more detailed quantitative examination in future studies.

For a weak deviation, $x = 0.1$, from half-filling, $n = 2.7 < 3$, the corresponding temperature dependence of the magnetic susceptibility (presented in the upper panel of Figure 9) is changed. Here, the electrons of the Mo network are still strongly correlated and nearly localized and, thus, support the same overall AFM order as for $x = 0$; however, the itinerant degrees of freedom viewed as holes with concentration $\delta n = 0.3$ can be readily spin-polarized by the external field, in contrast to the weaker response of the rigid localized AFM framework. Therefore, at $x = 0.1$, the magnetic susceptibility is the sum of two contributions, namely, a weaker one from the antiferromagnetically coupled localized moments and a somewhat larger contribution from the itinerant part.

As the Sr concentration x increases beyond 0.1, the magnetic response of the entire system continues to evolve. For $x = 0.3$, the neutron diffraction data provides definite evidence of the AFM state ($\mu_{AFM} = 2.9$ μ_B per site, $\mu_{FM} \approx 0$). Both the magnetic and neutron measurements for $x \geq 0.4$ indicate the advent of the other physical regime, which persists up to $x = 1$, as seen in the lower panels in Figure 9 (here, one has to pay attention to the larger scale for M/H compared to that of the upper panel).

The nominal charge difference between the Fe and Mo ions grows with x and makes dissimilar ions occupy alternative sublattices, A and B, and this kind of structural ordering is expected to increase as x increases. At $x = 1$, the highest possible charge disproportionation between the Fe^{3+} and Mo^{6+} ions dictates

the largest cation adjustment; one sublattice is fully occupied by Fe cations, and the residual Fe cations are randomly distributed in the second sublattice with the Fe spins on different sublattices connected through the NN AFM superexchange J_{FF}. Moreover, at $x = 1$, the magnetic Fe and nonmagnetic Mo networks are fully decoupled as the conduction band is empty, $n = 0$. We suggest that the value of the magnetic-ordering temperature in the Fe network is not far from the estimated $T'_N = 450$ K obtained earlier for the percolating infinite cluster of Fe cations. However, although the ordering in the percolating cluster with equal distribution of Fe ions over both sublattices is classified as the AFM one, the present case of $SrFe_{2/3}Mo_{1/3}O_3$ should be regarded as an insulating FIM pattern: most of the Fe ions with "up"-oriented magnetic moments occupy the A sublattice, and the remaining portion of the Fe cations with moments "down" are on the B sublattice. The increase of the measured susceptibility M/H below $T_C \approx 410$ K (at $x = 1$) indicates the onset of the FIM state. The atomic interchange between the A and B sublattices or the "up" and "down" spin alignment is considered to produce energetically equivalent FIM configurations, and this degeneracy may give rise to a domain structure in the sample.

Considering now the whole range $0.4 \le x \le 1$, one may see from the lower panels of Figure 9 that the characteristic temperature dependence of the magnetic susceptibility M/H measured at different x is qualitatively similar, and the onset of a magnetic ordering occurs in the same temperature interval between 410 and 450 K. This observation shows that the main features of the magnetic structure persist over a wide range of x, irrespective of the varying degree of B-cation order and changes to conduction-band occupancy, $0 \le n \le 2$. We conclude that the magnetic free energy of the dense Fe network dominates over the other sources of spin interactions in the whole system and determines the scale of the Fe core spin FIM ordering temperature $T_C \approx T'_N = 450$ K, as discussed previously. The ordered Fe core spins create alternating internal exchange fields on the sites of the Mo ions and polarize the spins of itinerant Mo electrons. The mechanism behind this polarization is the same as that in the standard double perovskites. A close inspection shows that the spin density at Mo located on the A(B) sublattice is up(down)-polarized, that is, this density follows the FIM arrangement imposed by the ordering of the Fe moments.

Recalling that the magnetically ordered phase is regarded to be the AFM one for $x \approx 0.1$ because of the complete cancellation of the sublattice magnetizations owing to the full cation structural disorder, there is no such cancelation for $x > 0.4$, and the system acquires a finite net magnetic moment, which signifies the FIM state. This conclusion is in compliance with the neutron magnetic scattering data. As discussed previously, in the representative sample with $x = 0.5$, the low-temperature measurements revealed the presence of both the FM and AFM components in the magnetic structure, compatible with the FIM state. The other argument in favour of the derived picture is the remarkable similarity with the temperature-dependent magnetic behaviour that is characteristic of the FIM phase in double perovskites, as reported in ref.[10] We refer to Figure 3 from ref.,[10] in which the data are presented for the magnetization $M(T)$ measured under an external magnetic field with x varied in the range $1/2 \le x \le 1$. A comparison with the corresponding data in the lower panels of Figure 9 reveals not only a qualitative similarity in the temperature dependence of the field-induced magnetization in both compounds but also that the onset of a magnetic ordering in them occurs at $T_C \approx 450$ K. The latter coincidence seems to be an accidental one, as the mechanisms behind the formation of FIM ordering in the two compounds are quite different.

Conclusions

The series of $La_{1-x}Sr_xFe_{2/3}Mo_{1/3}O_3$ solid solutions enables an exceptionally wide tuning of the 4d-element oxidation state with the 3d-element oxidation state virtually unchanged. The Fe oxidation state is close to +3 throughout the series, whereas the Mo oxidation state increases from +3 in the La-based compound ($x = 0$) to +6 in the Sr-based compound ($x = 1$). The charge difference between the Fe and Mo cations, which may result in the ordering of the B cations, becomes significant (>2) only for $x \ge 2/3$. Therefore, the magnetic behaviour of $La_{1-x}Sr_xFe_{2/3}Mo_{1/3}O_3$ ($0.0 \le x \le 0.7$) seems to be governed only by the multitude of various superexchange and double-exchange magnetic interactions between similar (Fe–Fe and Mo–Mo) and distinctly different (Fe–Mo) ions. In the vicinity of the $La_{1/3}Sr_{2/3}Fe_{2/3}Mo_{1/3}O_3$ composition, the saturation magnetization reaches its highest value $\mu_S \le 1$ μ_B, which corresponds to the formation of a ferrimagnetic state. The critical temperature of this state formation remains rather high ($T_c \approx 420$ K); therefore, this and neighbouring compounds are attractive for practical applications.

Experimental Section

General: Samples of $La_{1-x}Sr_xFe_{2/3}Mo_{1/3}O_3$ ($0 \le x \le 0.9$) were prepared by heating stoichiometric amounts of La_2O_3, Fe_2O_3, MoO_2, Mo metal and Sr_3MoO_6 at 1050–1150 °C in an Ar/H_2 (9 %) mixture. MoO_2 was prepared by the two-step reduction of MoO_3 in an Ar/H_2 (9 %) mixture at 500 °C for 7 h with final annealing at 700 °C for 7 h. Sr_3MoO_6 was synthesized by heating stoichiometric amounts of $SrCO_3$ and $SrMoO_4$ at 950 °C for 50 h. All used reagents were analytical grade. $SrFe_{2/3}Mo_{1/3}O_3$ was prepared by a citrate-based route. For the synthesis, excess citric acid monohydrate was melted in a porcelain cup, and stoichiometric amounts of $Sr(NO_3)_2$, $FeC_2O_4{\cdot}2H_2O$ and $(NH_4)_6Mo_7O_{24}{\cdot}4H_2O$ dissolved in a minimal amount of water were added. The mixture was heated in air until a dark solid formed. The obtained precursors were annealed preliminarily at 500 °C for 8 h and then pressed into pellets, and the samples were fired at 800 °C for 8 h. The final heat treatment was performed in an Ar/H_2 (9 %) mixture at 1000–1150 °C for 24 h.

The phase-purities of the compounds were checked by XRPD with a Huber G670 Guinier diffractometer (Cu-$K_{\alpha 1}$ radiation, image foil detector). The TG studies were performed in artificial air [20 % O_2, 80 % Ar] from 25 to 900 °C at a heating rate of 10 K/min with a Netzsch STA 449C thermoanalyzer.

The NPD data for $La_{0.7}Sr_{0.3}Fe_{2/3}Mo_{1/3}O_3$ and $La_{0.5}Sr_{0.5}Fe_{2/3}Mo_{1/3}O_3$ were collected with a high-resolution Fourier diffractometer[36] at the IBR-2 pulsed reactor in Dubna. The correlation method for data

collection with the high-resolution Fourier diffractometer provides an exceptionally high resolution ($\Delta d/d \approx 0.001$), which is practically independent of the interplanar distance over a wide range of d_{hkl}. The Rietveld analysis of the diffraction patterns was performed with the MRIA[37] and FullProf[38] program packages with the use of their internal tables for coherent scattering lengths and magnetic form factors.

The XANES studies of $La_{1-x}Sr_xFe_{2/3}Mo_{1/3}O_3$ ($0 \le x \le 1$) were performed at beamlines 17C and 01C at the National Synchrotron Radiation Research Center in Taiwan. To study the oxidation states of the cations, Fe-*K*-edge and Mo-*K*-edge XANES spectra were recorded in transmission mode at room temperature. The energy resolution of the Fe-*K*-edge spectra was 0.35 eV, and that of the Mo-*K*-edge spectra was 1 eV.

The magnetization of $La_{1-x}Sr_xFe_{2/3}Mo_{1/3}O_3$ pellet samples was studied with a Quantum Design PPMS-9T physical properties measurement system in the temperature range 2–1000 K under a magnetic field of up to 9 T.

Acknowledgments

The work was supported by Act 211 of the Government of the Russian Federation, contract number 02.A03.21.0006, the Ministry of Education and Science of the Russian Federation in the framework of Increase Competitiveness Program of NUST "MISiS", contract number K4-2015-020, the grants-in-aid of the Ministry of Education and Science of Russia (MK-3443.2013.2), and the Russian Foundation for Basic Research (project numbers 12-03-00665, 13-02-00050, 13-02-00374, 14-02-00111, 14-02-00245 and 14-02-92002). The neutron part of this study was performed with financial support from the Russian Science Foundation (project number 14-12-00896). S. Ya. I. acknowledges the Russian Science Foundation (project number 16-13-10327) for the financial support.

Keywords: Perovskite phases · Magnetic properties · Iron · Molybdenum

[1] K.-I. Kobayashi, T. Kimura, H. Sawada, K. Terakura, Y. Tokura, *Nature* **1998**, *395*, 677.
[2] S. A. Wolf, D. D. Awschalom, R. A. Buhrman, J. M. Daughton, S. von Molnar, M. L. Roukes, A. Y. Chtchelkanova, D. M. Treger, *Science* **2001**, *294*, 1488.
[3] J. M. D. Coey, C. L. Chien, *MRS Bull.* **2003**, *28*, 720.
[4] H. Y. Hwang, S.-W. Cheong, N. P. Ong, B. Batlogg, *Phys. Rev. Lett.* **1996**, *77*, 2041.
[5] M. Imada, A. Fujimori, Y. Tokura, *Rev. Mod. Phys.* **1998**, *70*, 1039.
[6] D. Serrate, J. M. De Teresa, M. R. Ibarra, *J. Phys. Condens. Matter* **2007**, *19*, 023201.CCDC 023201 (for **XX1**) contains the supplementary crystallographic data for this paper. These data can be obtained free of charge from The Cambridge Crystallographic Data Centre.
[7] D. Sánchez, J. A. Alonso, M. García-Hernández, M. J. Martínez-Lope, J. L. Martínez, A. Mellergård, *Phys. Rev. B* **2002**, *65*, 104426.
[8] J. Linden, T. Yamamoto, M. Karppinen, H. Yamauchi, T. Pietari, *Appl. Phys. Lett.* **2000**, *76*, 2925.
[9] J.-S. Kang, J. H. Kim, A. Sekiyama, S. Kasai, S. Suga, S. W. Han, K. H. Kim, T. Muro, Y. Saitoh, C. Hwang, C. G. Olson, B. J. Park, B. W. Lee, J. H. Shim, J. H. Park, B. I. Min, *Phys. Rev. B* **2002**, *66*, 113105.
[10] J. Navarro, C. Frontera, L. Balcells, B. Martínez, J. Fontcuberta, *Phys. Rev. B* **2001**, *64*, 092411.
[11] C. Frontera, D. Rubi, J. Navarro, J. L. García-Munõz, J. Fontcuberta, C. Ritter, *Phys. Rev. B* **2003**, *68*, 012412.
[12] A. Kahoul, A. Azizi, S. Colis, D. Stoeffler, R. Moubah, G. Schmerber, C. Leuvrey, A. Dinia, *J. Appl. Phys.* **2008**, *104*, 123903.
[13] J. Linden, T. Shimada, T. Motohashi, H. Yamauchi, M. Karppinen, *Solid State Commun.* **2004**, *129*, 129.
[14] R. D. Shannon, *Acta Crystallogr., Sect. A* **1976**, *32*, 751.
[15] P. Sanyal, H. Das, T. Saha-Dasgupta, *Phys. Rev. B* **2009**, *80*, 224412.
[16] H. Wu, R. Lu, W. Tan, C. Xiao, K. Deng, Y. Qian, *Appl. Phys. Lett.* **2012**, *100*, 132404.
[17] A. A. Markov, I. A. Leonidov, M. V. Patrakeev, V. L. Kozhevnikov, O. A. Savinskaya, U. V. Ancharova, A. P. Nemudry, *Solid State Ionics* **2008**, *179*, 1050.
[18] G. Y. Liu, G. H. Rao, X. M. Feng, H. F. Yang, Z. W. Ouyang, W. F. Liu, J. K. Liang, *J. Alloys Compd.* **2003**, *353*, 42.
[19] D. Topwal, D. D. Sarma, H. Kato, Y. Tokura, M. Avignon, *Phys. Rev. B* **2006**, *73*, 094419.
[20] S. R. Popuri, D. Redpath, G. Chan, R. I. Smith, O. Cespedes, J.-W. G. Bos, *Dalton Trans.* **2015**, *44*, 10621.
[21] O. N. Meetei, O. Erten, A. Mukherjee, M. Randeria, N. Trivedi, P. Woodward, *Phys. Rev. B* **2013**, *87*, 165104.
[22] O. Erten, O. N. Meetei, A. Mukherjee, M. Randeria, N. Trivedi, P. Woodward, *Phys. Rev. B* **2013**, *87*, 165105.
[23] O. Erten, O. N. Meetei, A. Mukherjee, M. Randeria, N. Trivedi, P. Woodward, *Phys. Rev. Lett.* **2011**, *107*, 257201.
[24] G. V. Bazuev, V. G. Zubkov, G. P. Shveikin, *Russ. J. Inorg. Chem.* **1996**, *41*, 1895.
[25] M. C. Viola, J. A. Alonso, J. C. Pedregosa, R. E. Carbonio, *Eur. J. Inorg. Chem.* **2005**, 1559.
[26] C. A. Lopez, M. C. Viola, J. C. Pedregosa, J. A. Alonso, M. T. Fernández-Díaz, *Eur. J. Inorg. Chem.* **2010**, 4110.
[27] M. T. Anderson, K. B. Greenwood, G. A. Taylor, K. R. Poeppelmeier, *Prog. Solid State Chem.* **1993**, *22*, 197.
[28] T. Ressler, J. Wienold, R. E. Jentoft, T. Neisius, *J. Catal.* **2002**, *210*, 67.
[29] J. R. Hayes, A. P. Grosvenor, *J. Alloys Compd.* **2012**, *537*, 323.
[30] F. de Groot, G. Vankó, P. Glatzel, *J. Phys. Condens. Matter* **2009**, *21*, 104207.
[31] J. L. Alonso, L. A. Fernández, F. Guinea, F. Lesmes, V. Martín-Mayor, *Phys. Rev. B* **2003**, *67*, 214423.
[32] S. Vasala, M. Karppinen, *Prog. Solid State Chem.* **2015**, *43*, 1.
[33] Y. Tomioka, T. Okuda, Y. Okimoto, R. Kumai, K.-I. Kobayashi, Y. Tokura, *Phys. Rev. B* **2000**, *61*, 422.
[34] A. Georges, L. de'Medici, J. Mravlje, *Annual Rev. Cond. Matt. Phys.* **2013**, *4*, 137.
[35] R. B. Stinchcombe, *J. Phys. C: Solid State Phys.* **1979**, *12*, 4533.
[36] A. M. Balagurov, *Neutron News* **2005**, *16*, 8.
[37] V. B. Zlokazov, V. V. Chernyshev, *J. Appl. Crystallogr.* **1992**, *25*, 447.
[38] J. Rodriguez-Carvajal, *Phys. B* **1993**, *192*, 55.

Received: January 10, 2016
Published Online: ■

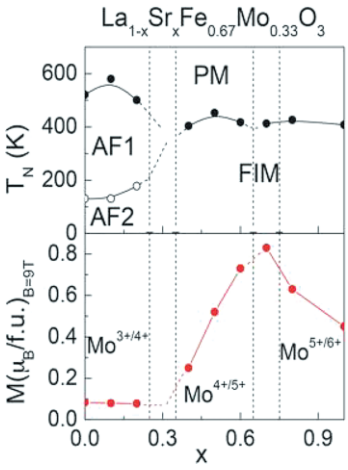

$La_{1-x}Sr_xFe_{2/3}Mo_{1/3}O_3$ perovskites allow wide tuning of the Mo oxidation state from +3 (x = 0) to +6 (x = 1) with the Fe^{III} oxidation state virtually unchanged. The magnetic properties vary between antiferromagnetic (AFM) for x = 0 to ferromagnetic (FIM) for x = 1.0.

DOI: 10.1002/ejic.201600020